LETTERS

Notch and EGFR pathway interaction regulates neural stem cell number and self-renewal

Adan Aguirre[1]†, Maria E. Rubio[2] & Vittorio Gallo[1]

Specialized cellular microenvironments, or 'niches', modulate stem cell properties, including cell number, self-renewal and fate decisions[1,2]. In the adult brain, niches that maintain a source of neural stem cells (NSCs) and neural progenitor cells (NPCs) are the subventricular zone (SVZ) of the lateral ventricle and the dentate gyrus of the hippocampus[3–5]. The size of the NSC population of the SVZ at any time is the result of several ongoing processes, including self-renewal, cell differentiation, and cell death. Maintaining the balance between NSCs and NPCs in the SVZ niche is critical to supply the brain with specific neural populations, both under normal conditions or after injury. A fundamental question relevant to both normal development and to cell-based repair strategies in the central nervous system is how the balance of different NSC and NPC populations is maintained in the niche. EGFR (epidermal growth factor receptor) and Notch signalling pathways have fundamental roles during development of multicellular organisms[6]. In *Drosophila* and in *Caenorhabditis elegans* these pathways may have either cooperative or antagonistic functions[7–9]. In the SVZ, Notch regulates NSC identity and self-renewal, whereas EGFR specifically affects NPC proliferation and migration[10–13]. This suggests that interplay of these two pathways may maintain the balance between NSC and NPC numbers. Here we show that functional cell–cell interaction between NPCs and NSCs through EGFR and Notch signalling has a crucial role in maintaining the balance between these cell populations in the SVZ. Enhanced EGFR signalling *in vivo* results in the expansion of the NPC pool, and reduces NSC number and self-renewal. This occurs through a non-cell-autonomous mechanism involving EGFR-mediated regulation of Notch signalling. Our findings define a novel interaction between EGFR and Notch pathways in the adult SVZ, and thus provide a mechanism for NSC and NPC pool maintenance.

We examined whether changes in SVZ NPC number affect NSC properties. In the mouse expressing the human EGFR under control of the *Cnp* promoter (*Cnp*–hEGFR) , the hEGFR is expressed in *Cnp*-expressing NPCs and in NG2$^+$ progenitors[14,15], but not in *GFAP*-expressing NSCs or in neuroblasts (Supplementary Fig. 1a, b). EGFR overexpression enhances EGFR signalling in the adult SVZ (data not shown) and expands the NPC pool[14,15] (Supplementary Fig. 1a, b). The SVZ of *Cnp*–hEGFR mouse contains more NG2$^+$ progenitors than wild type, but a reduced number of GFAP$^+$ NSCs (Fig. 1a and Supplementary Fig. 2). In wild type, GFAP$^+$ cells show a radial glia-like morphology (Supplementary Fig. 1c panel 1), whereas in *Cnp*–hEGFR mice GFAP$^+$ cells show a morphology of protoplasmatic astrocytes (Supplementary Fig. 1d panel 1)[16]. GFAP and Nestin were co-expressed in the wild-type SVZ, whereas the percentage of GFAP$^+$Nestin$^+$ cells was reduced in *Cnp*–hEGFR mice (Fig. 1a, b).

In SVZ cells from *Cnp*–hEGFR mice, Lex$^+$Nestin$^+$GFAP$^+$ NSCs were reduced, compared to wild type (Fig. 1a, b). This was not due to cell death (0.6 ± 0.02 and 0.5 ± 0.06% of Caspase3$^+$ cells per 10^6 μm^3, wild type and *Cnp*–hEGFR, respectively). Ultrastructural analysis[17] confirmed fewer NSCs and more neuroblasts in *Cnp*–hEGFR mice compared to wild type (Supplementary Fig. 3).

We used LeX antibodies[18,19] to FACS-purify LeX$^+$ *Cnp*–EGFP^{neg} SVZ NSCs from *Cnp*–EGFP (*Cnp* promoter-driven enhanced green fluorescent protein) and *Cnp*–EGFP/*Cnp*–hEGFR mice (Supplementary Fig. 4). LeX$^+$ *Cnp*–EGFP^{neg} cells were GFAP$^+$ (data not shown). The number of LeX$^+$ *Cnp*–EGFP^{neg} NSCs was reduced in the *Cnp*–hEGFR mouse, whereas LeX$^+$ *Cnp*–EGFP$^+$ NPCs were increased (Supplementary Fig. 4). LeX$^+$ *Cnp*–EGFP^{neg} NSCs from *Cnp*–hEGFR mice had a reduction in LeX$^+$ neurosphere[19,20] number and size, compared to wild-type cells (Fig. 1c, d). Conversely, *Cnp*–EGFP$^+$LeX$^+$ NPC proliferation was increased (not shown).

In *GFAP*–GFP/*Cnp*–hEGFR mice, *GFAP*–GFP$^+$ (encoding a GFAP–green fluorescent protein fusion) cells with radial glia-like morphology

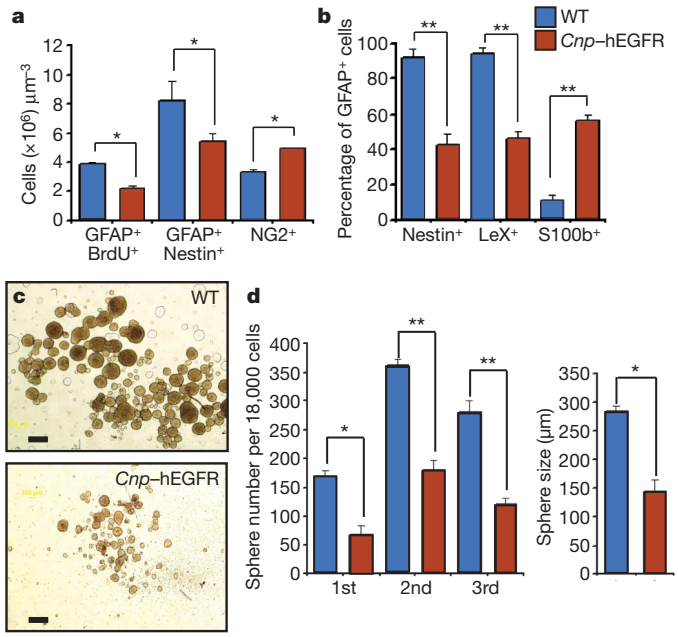

Figure 1 | EGFR overexpression reduces NSC proliferation and self renewal in the adult mouse SVZ. a, Decreased number of GFAP$^+$BrdU$^+$ and GFAP$^+$Nestin$^+$ NSCs, and increased number of NG2$^+$ cells in the SVZ of the *Cnp*–hEGFR mouse (*$P < 0.05$). Means ± s.e.m. **b**, Decreased percentage of GFAP$^+$Nestin$^+$LeX$^+$ NSCs and increased percentage of GFAP$^+$S100b$^+$ astrocytes in the SVZ of the *Cnp*–hEGFR mouse (**$P < 0.02$). **c**, Neurospheres from wild-type (WT) and *Cnp*–hEGFR cells. Scale bars, 50 μm. **d**, Reduced neurosphere numbers and size in cultures from *Cnp*–hEGFR mice (*$P < 0.02$; **$P < 0.001$).

[1]Center for Neuroscience Research, Children's National Medical Center, Washington, District of Columbia 20010, USA. [2]University of Pittsburgh Medical School, Department Otolaryngology, Pittsburgh, Pennsylvania 15261, USA. †Present address: SUNY at Stony Brook University, Pharmacology Department, Stony Brook, New York 11794-5140, USA.

were almost absent in the SVZ (Supplementary Fig. 5b). Conversely, in *GFAP*–GFP mice, GFP$^+$ cells displayed radial glia-like cell morphology throughout the SVZ (Supplementary Fig. 5a). In FACS-purified cells from *GFAP*–GFP and *GFAP*–GFP/*Cnp*–hEGFR mice, enhanced EGFR signalling reduced the number of LeX$^+$*GFAP*–GFP$^+$ NSCs, whereas the number of LeX$^+$*GFAP*–GFP^{neg} NPCs was increased (Supplementary Fig. 5c, d). NSCs from *GFAP*–GFP/*Cnp*–hEGFR mice displayed reduced neurosphere number and size compared to cells from *GFAP*–GFP mice (Supplementary Fig. 5c, d); however, proliferation of LeX$^+$*GFAP*–GFP^{neg} NPCs was increased (not shown). These results show that enhanced EGFR signalling and expansion of SVZ *Cnp*-expressing progenitors[14,15] reduces the number, proliferation and self-renewal of *GFAP*-expressing NSCs.

Notch[10,21,22], BMP[23,24] and Shh[25] regulate NSC properties in the SVZ. Enhanced EGFR signalling upregulated genes involved in neurogenesis (Supplementary Table 1 (GEO access number GSE21913) and Fig. 2a), whereas Notch signalling elements were downregulated. Shh and BMP pathways were not modified (data not shown). In wild-type and *Cnp*–hEGFR SVZ Notch1 was mainly detected in NSCs[22,26], whereas Dll1 and Jagged1 were detected in NPCs and in neuroblasts (Supplementary Fig. 6a–f; see also Fig. 4a–d). *Dll*–EGFP electroporation demonstrated expression in EGFR$^+$NG2$^+$ and in Dcx$^+$ cells, but not in GFAP$^+$ cells (Supplementary Fig. 6g–j). Conversely, *Hes1* activity was mainly observed in GFAP$^+$ cells (Supplementary Fig. 6k–m; see also Fig. 4a–d). Notch1, NICD (Notch1 intracellular domain), Dll1, RBPJK and Hes1 proteins were decreased by 60 ± 3, 63 ± 4, 20 ± 2, 30 ± 2.5 and 40 ± 3% upon enhanced EGFR function, respectively (n = 3–4 each; Fig. 2a). Conversely, Numb was increased by 45 ± 3% (n = 3). In the SVZ of the Wa2 mouse[14], NPC number and proliferation were reduced[27], and Notch1, NICD, RBPJK and Hes1 were upregulated, compared to wild type (Fig. 2b).

EGF infusion into the lateral ventricle of *GFAP*–GFP mice increased the number of 5-bromo-2-deoxyuridine-positive (BrdU$^+$) cells in the SVZ, downregulated Notch signalling and expanded EGFR-expressing NPCs (Supplementary Fig. 7a–e). Proliferation and self-renewal of NSCs from EGF-infused SVZ were reduced compared to controls (Supplementary Fig. 7f, g).

To rescue the NSC phenotype in the postnatal *Cnp*–hEGFR mice, we overexpressed the constitutively active form of Notch1 (NICD) in *Cnp*–hEGFR SVZ cells (Supplementary Fig. 8a). Neurosphere numbers and size were greater in *NICD*-transfected than in mock-transfected cells (Supplementary Fig. 8b). *NICD* electroporation in SVZ cells of *Cnp*–hEGFR/*GFAP*–GFP mice partially rescued the radial glia-like morphology of *GFAP*-expressing cells (Fig. 2c, d; see also Fig. 4a panels 1–3 and 4b panels 1–3), and increased neurosphere number and size (Fig. 2e, f). After adenovirus-mediated transduction of *NICD* (Fig. 2g) in adult wild-type and *Cnp*–hEGFR mice, NICD levels were higher (30 ± 3%) in *NICD*-LacZ-infected (Ad-*NICD*) than in LacZ adenovirus (Ad-LacZ)-infected SVZs, whereas Numb levels were reduced (55 ± 4%) (Fig. 2h). *NICD* transduction rescued NSC properties in the SVZ of *Cnp*–hEGFR/*GFAP*–GFP mice (Fig. 2h, i).

We infused cytosine-β-D-arabinofuranoside (Ara-C) into the lateral ventricle to deplete dividing NPCs[9]. In saline-perfused adult mice, BrdU$^+$ cell number was significantly higher in *Cnp*–hEGFR mice (24.1 ± 2.1 cells per 10^6 μm^3) compared to wild type (12.4 ± 0.5 cells per 10^6 μm^3) (Supplementary Fig. 9a, b; t-test $P < 0.008$), whereas NSC number was reduced (Supplementary Fig. 9a, b and Fig. 3a; t-test $P < 0.005$). Ara-C increased GFAP$^+$ cell number in the SVZ of adult *Cnp*–hEGFR mice (Supplementary Fig. 9c, d and Fig. 3a). We observed higher levels of Notch1 in GFAP$^+$ NSCs of Ara-C-treated *Cnp*–hEGFR and wild-type mice, compared with saline-infused mice (not shown). In *Cnp*–hEGFR mice, *Hes1* and *RBPjk* mRNAs and Notch1 protein

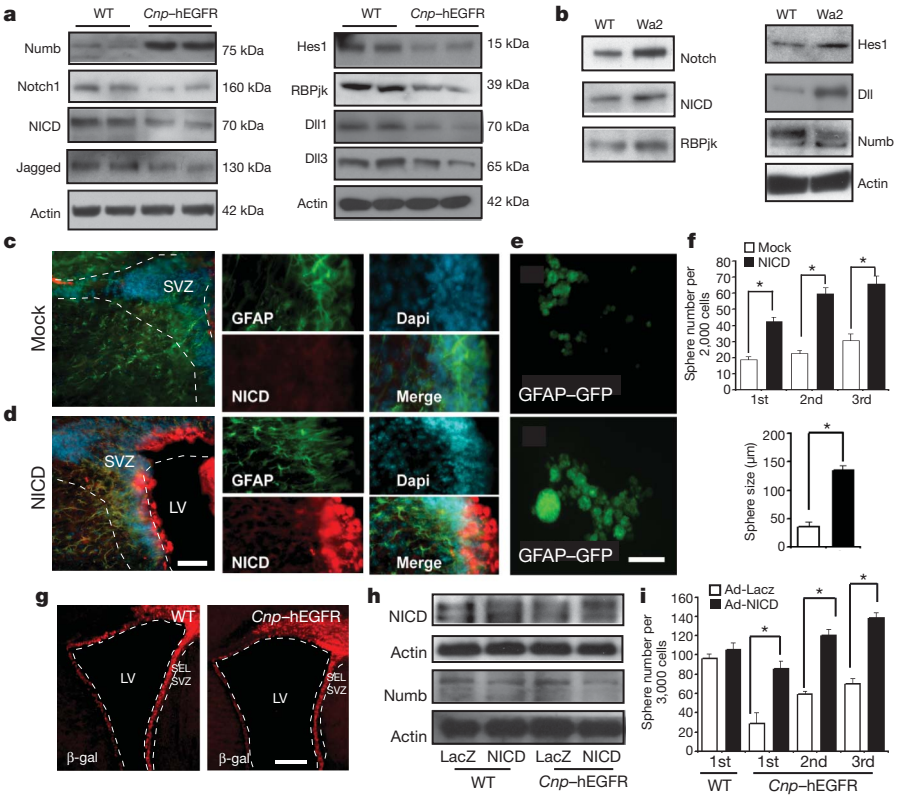

Figure 2 | EGFR overexpression downregulates Notch signalling in the SVZ, and NICD overexpression rescues proliferation and self-renewal of SVZ NSCs. **a**, Notch signalling is downregulated, but Numb is upregulated in the SVZ of *Cnp*–hEGFR mice. **b**, NICD, RBPjk, Hes1 are upregulated in the Wa2 SVZ, and Numb is downregulated. **c**, **d**, High NICD levels were detected after *in vivo* electroporation by immunostaining. **e**, **f**, GFAP–GFP$^+$ neurosphere number (top) and size (bottom) increased after *NICD* electroporation. Means (n = 3) ± s.e.m. (*$P < 0.01$). Scale bars, 100 μm. **g**, High β-gal expression levels in the SVZ after viral infection in wild-type and *Cnp*–hEGFR ventricles. LV, lateral ventricle. **h**, Ad-*NICD* transduction increased NICD, but reduced Numb expression. **i**, Ad-*NICD* infection increased neurosphere formation in *Cnp*–hEGFR mice, but not in wild type. Means (n = 3) ± s.e.m. (*$P < 0.02$). Scale bars, 200 μm.

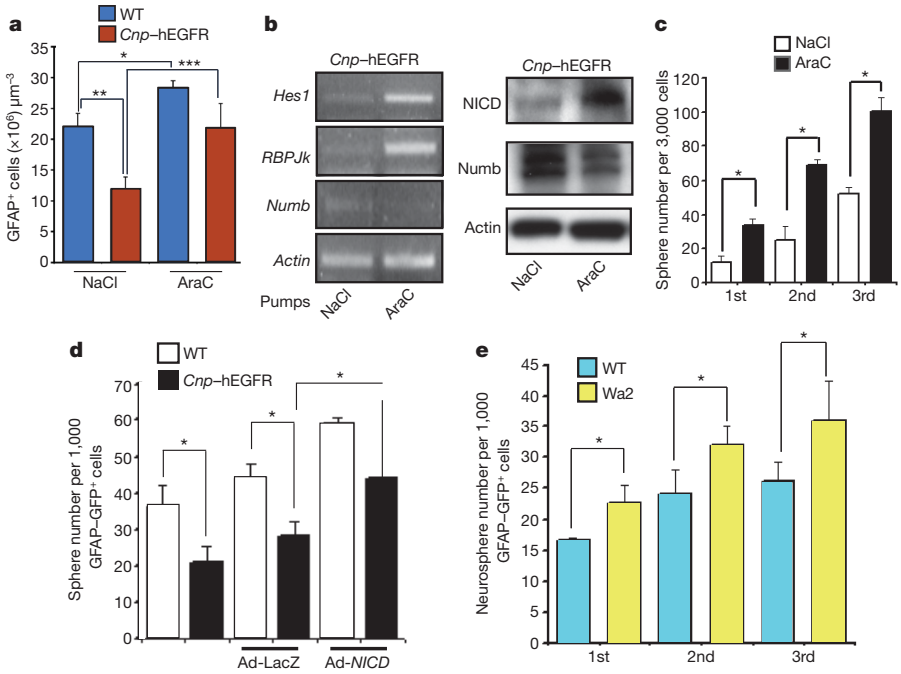

Figure 3 | EGFR-expressing NPCs regulate NSC properties through a non-autonomous cellular mechanism. **a**, Increased BrdU$^+$ cells and reduced GFAP$^+$ cells in *Cnp*–hEGFR mice (**$P < 0.002$). AraC: Increased GFAP$^+$ cells compared with NaCl in *Cnp*–hEGFR mice (**$P < 0.002$; *$P < 0.05$). **b**, left, AraC upregulates *Hes1* and *RBPjk* mRNAs and downregulates *Numb*. **b**, right, AraC upregulates NICD protein and downregulates Numb. **c**, *Cnp*–hEGFR mice: AraC increases NSC proliferation and self-renewal (*$P < 0.001$). Means ($n = 3$) ± s.e.m. **d**, Reduced proliferation and self-renewal in wild-type NSCs grown with *Cnp*–hEGFR NPCs, as compared with wild-type cells. Ad-*NICD* overexpression rescued NSC proliferation. Means ($n = 3$) ± s.e.m. (*$P < 0.02$). **e**, Higher proliferation and self-renewal of NSCs cultured with NPCs of the Wa2 mouse, as compared with wild-type cells. Means ($n = 3$) ± s.e.m. (*$P < 0.05$).

levels were higher in Ara-C-treated SVZ tissues than in saline controls (Fig. 3b), whereas *Numb* mRNA and protein were reduced (Fig. 3b). Cell proliferation and self-renewal were enhanced in neurospheres from Ara-C-treated tissue, compared with saline (Fig. 3c). Altogether, these data indicate that NPCs regulate NSC proliferation and self-renewal *in vivo*.

To demonstrate that contact with NPCs regulates NSC proliferation and self-renewal through Notch, we co-cultured confluent SVZ NPCs from wild-type or *Cnp*–hEGFR mice with NSCs FACS-purified from *GFAP*–GFP mice (Supplementary Fig. 10). *GFAP*–GFP$^+$ NSCs were then FACS-purified from these co-cultures. Notch signalling was downregulated in NSCs co-cultured with *Cnp*–hEGFR NPCs, and cell proliferation and self-renewal were reduced (Fig. 3d and Supplementary Fig. 10c). NICD transduction partially rescued this phenotype (Fig. 3d). In NSCs FACS-purified from Wa2 NPC/wild-type NSC co-cultures, Notch signalling and neurosphere formation were enhanced, as compared to wild-type NPC/wild-type NSC in NSCs (Fig. 3e and Supplementary Fig. 10f). These results confirm that EGFR regulates Notch through a non-cell-autonomous mechanism.

We determined whether EGFR regulates the Notch pathway and investigated the molecular mechanism. In transfected SVZ cells, *CBF-1* and *Hes1* promoter activity was higher in wild-type than in *Cnp*–hEGFR cells, even after *NICD* co-transfection (Supplementary Fig. 11a). In wild-type cells, *Hes1* activity was enhanced by *NICD* and reduced after *hEGFR* co-transfection (Supplementary Fig. 11b). *hEGFR* co-transfected with different *Notch* constructs (Supplementary Fig. 11c) reduced *Hes1* activation (Supplementary Fig. 11d), and the EGFR inhibitor PD168393 (ref. 15) restored *Hes1* activity (Supplementary Fig. 11e). *Cnp*–hEGFR cells plated on wild-type cells transfected with *Hes1*-luciferase suppressed basal *Hes1* activity; this effect was reversed by PD168393 (Supplementary Fig. 11f). Finally, *Hes1* promoter activity was higher in Wa2 SVZ cells than in wild-type cells (Supplementary Fig. 11g).

We electroporated Notch target constructs (Supplementary Fig. 12) to identify SVZ Notch-responsive cells and to elucidate the mechanism of Notch regulation. *Hes1* activity was observed in NSCs (Fig. 4a–d and Supplementary Fig. 12m, n), and was found in a larger percentage of *GFAP*–GFP$^+$ cells (47.8 ± 3.6 cells µm^{-3}) than in *GFAP*–GFP$^+$/*Cnp*–hEGFR$^+$ cells (23.6 ± 4.6 cells µm^{-3}, $P < 0.01$). Similar results were observed with *CBFRE*–GFP and *Hes5*–GFP (Supplementary Fig. 12a–l and o–r). *Hes1* activity in NSCs of *GFAP*–GFP/*Cnp*–hEGFR mice was rescued by *NICD* co-electroporation (66.5 ± 71 cells µm^{-3}, $P < 0.01$; $n = 4$). In Wa2 mice, a larger percentage of SVZ NSCs displayed *Hes1* and *CBFRE* activity, compared to wild type (Supplementary Fig. 13a–c, and not shown). shRNA-mediated knockdown of *hEGFR* in *Cnp*–hEGFR mice *in vivo* caused upregulation of Notch1 and Hes1 (Supplementary Fig. 13d, e). Consistent with these results, *Dll*–EGFP electroporation revealed a larger percentage of *Dll*–EGFP$^+$ cells in the SVZ of the wild-type mouse, compared to *Cnp*–hEGFR mouse (Supplementary Fig. 14). Altogether, our findings demonstrate that EGFR is an upstream regulator of Notch through a non-autonomous cellular mechanism.

Numb interacts with E3 ubiquitin ligases to regulate Notch receptor degradation[28]. Changes in Notch signalling levels directly regulate Numb expression[29]. Figure 4e shows that *NICD* overexpression reduced Numb in SVZ cells, whereas EGFR overexpression upregulated Numb, and reduced Notch1 and NICD levels. The Notch inhibitor DAPT upregulated Numb (Fig. 4f).

We determined the extent of Numb/Notch1 interaction in the SVZ by immunoprecipitation assays. Higher levels of Notch1 associated with Numb in *Cnp*–hEGFR samples, compared to wild type (Fig. 4g, left panel). Anti-ubiquitin immunoprecipitation followed by anti-Notch1 immunoblotting demonstrated higher levels of Notch ubiquitination in *Cnp*–hEGFR mice (Fig. 4g, right panel). Stereotaxic injection in wild-type and *Cnp*–hEGFR mice with either Ad-LacZ or *NICD*-LacZ adenovirus showed that both Numb–Notch interaction and Notch1 ubiquitination were reduced after NICD transduction (Fig. 4h).

To demonstrate that EGFR signalling promotes Notch ubiquitination via Numb, we performed gain- and loss-of-function experiments in SVZ cultures. After EGFR transfection, we observed

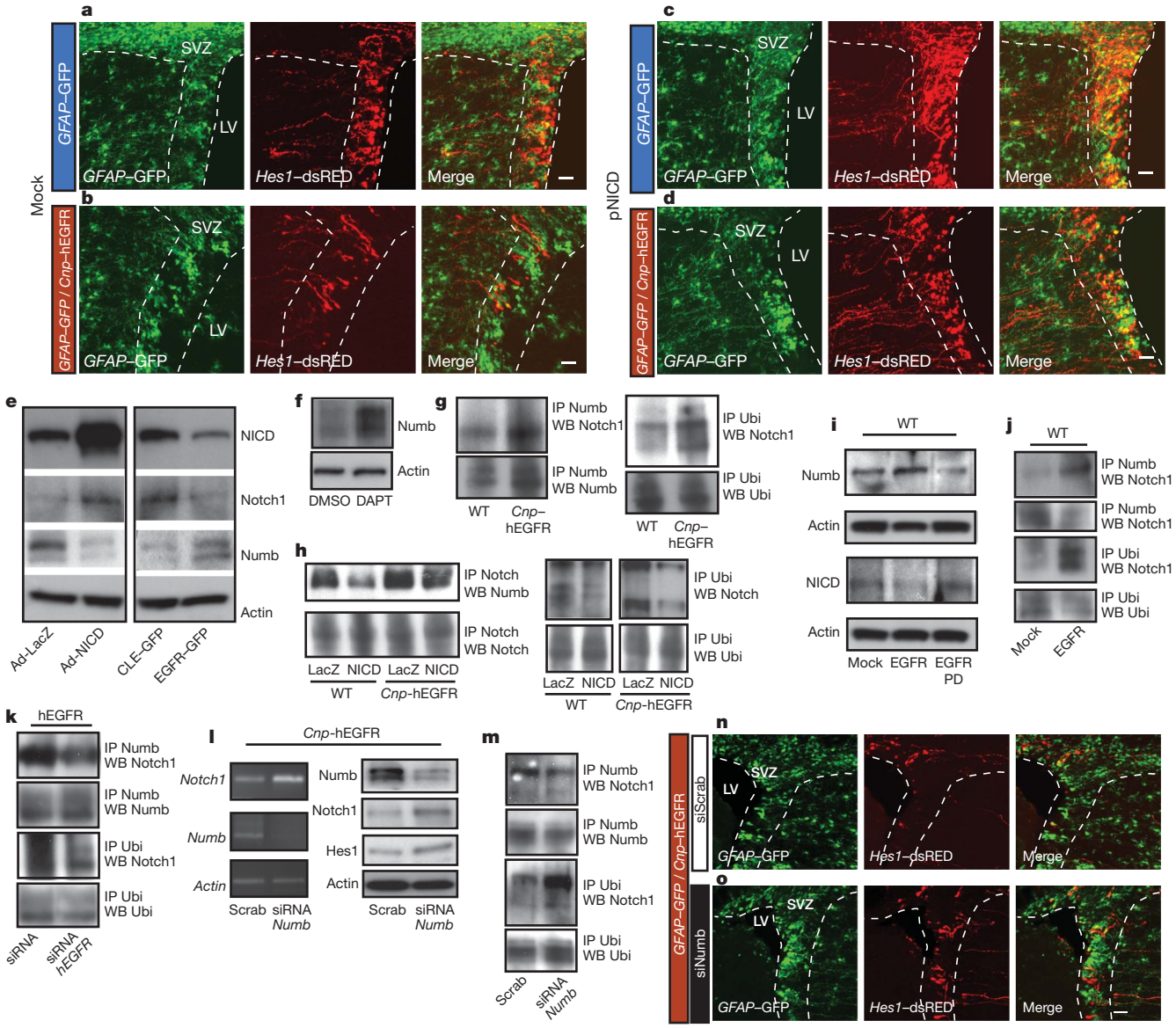

Figure 4 | EGFR signalling reduces Notch1 expression through Numb. **a**–**d**, *Hes1*-dsRED-*NICD* co-electroporation in *GFAP*–GFP (**a**, **c**)and *GFAP*–GFP/*Cnp*–hEGFR (**b**, **d**) mice. More *Hes1*-dsRED$^+$*GFAP*–GFP$^+$ cells are observed in *GFAP*–GFP mice. *NICD* increases *GFAP*–GFP$^+$*Hes1*-dsRED$^+$ cell number. **e**, Wild-type cells infected with LacZ, *NICD*, GFP retrovirus (*CLE*–GFP) or *EGFR*–GFP. *NICD* upregulates NICD and Notch1, but downregulates Numb. *EGFR* reduces Notch1 and NICD, but increases Numb. **f**, DAPT upregulates Numb. **g**, Increased Numb/Notch1 immunoprecipitation correlates with enhanced degradation. **h**, Ad-*NICD* reduces Notch1/Numb interaction and Notch1 degradation in *Cnp*–hEGFR SVZ. **i**, *EGFR* increases Numb and reduces NICD; PD168393 prevents these effects. **j**, *EGFR* increases Numb/Notch immunoprecipitation, and Notch1 degradation. **k**, *hEGFR* siRNAs decrease Numb/Notch1 interaction and Notch1 degradation in *Cnp*–hEGFR cells. **l**–**o**, *Numb* siRNA knockdown enhances Notch signalling in *Cnp*–hEGFR NSCs. Scrab, scrambled siRNA. **l**, *Numb* siRNA downregulates Numb and upregulates Notch1. **m**, *Numb* siRNA decreases Numb/Notch interaction and Notch1 degradation. **n**, **o**, Co-electroporation of Scrab (**n**) or *Numb* siRNA (**o**) with *Hes1*-dsRED constructs. *Numb* siRNA increases the number of *Hes1*-dsRED$^+$*CAG*–GFP$^+$ cells. Scale bars, 50 μm.

increased Numb levels and reduced NICD expression, compared to the mock construct (Fig. 4i). PD168393 reversed this effect (Fig. 4i). EGFR overexpression in wild-type cells promoted Numb and Notch association and enhanced Notch1 ubiquitination (Fig. 4j). siRNA-mediated EGFR knock-down in *Cnp*–hEGFR SVZ cultures reduced Numb and Notch1 interaction (Fig. 4k, top two panels), and decreased Notch1 ubiquitination (Fig. 4k, bottom two panels).

To confirm the role of EGFR and Numb in inhibiting Notch, we analysed *Hes1* promoter activity by co-transfection in wild-type SVZ cells with a *Hes1*-luciferase reporter construct, along with *hEGFR* and *Numb* expression vectors. *Hes1* activity was activated only by the *NICD* construct (Supplementary Fig. 11h). However, *Numb* blocked *NICD* and reduced *Hes1* activity (Supplementary Fig. 11h). *Hes1* activity was reduced further by co-transfection with *NICD*, *Numb* and *hEGFR* (Supplementary Fig. 11h). Finally, siRNA-mediated knockdown of *Numb in vivo* caused upregulation of *Notch1* and *Hes1* activity (Fig. 4l–o). Scrambled siRNA electroporation *in vivo* showed that *Hes1* activity was present in a small percentage of GFAP$^+$ and Nestin$^+$ NSCs (Fig. 4n; 3.9 ± 0.51 cells μm^{-3}); however, after *Numb* knock down *Hes1* activity was present in a larger percentage NSCs (Fig. 4o; 7.1 ± 0.56 cells μm^{-3}, $P < 0.01$; $n = 4$). Together, these results demonstrate that EGFR signalling reduces Notch activation through Numb-dependent Notch1 ubiquitination.

Our results point to an interaction between two signalling pathways, EGFR and Notch, that have fundamental and selective roles in the maintenance of NSCs and NPCs in the SVZ niche. This interplay occurs through the direct interaction between NPCs and NSCs, demonstrating the existence of a cellular homeostatic mechanism that involves two specific molecular pathways. Our study also proves that altering particular signalling mechanisms in selective cell types of the

SVZ can cause profound changes in the overall cell composition of this neurogenic region of the adult brain. Defining interactions and homeostatic mechanisms that occur between different types of SVZ cells under normal conditions provides crucial information on possible alterations of specific signalling pathways that might occur under pathological conditions or after brain injury.

METHODS SUMMARY

Generation/genotyping of *Cnp*–hEGFR, *hGFAP*–GFP and Wa2 mice was performed as described[14,15]. Wild-type C57/Bl6 and FVB/N mice were used as controls. Histology, immunohistochemistry and electron microscopy studies were performed on fresh floating or vibratome sections as described previously[19,20]. Immunohistochemistry and confocal imaging were used to characterize the SVZ cell composition of the postnatal and adult brain. Image analysis, three-dimensional rendering, and cell counting were done in Photoshop (Adobe) and ImageJ software. NSCs and NPCs were isolated and characterized by FACS sorting using anti-CD15, -GFAP, -EGFR and -NG2 antibodies. Cell proliferation, self-renewal and biochemical analysis were performed from FACS-purified cultured cells and SVZ tissue. To compare SVZ expression profiles of genes involved in NSC development/neurogenesis in *Cnp*–hEGFR and wild-type mice, we performed gene array (SuperArray) expression on spotted cDNA fragments encoding 250 mouse genes. To monitor the Notch-signalling pathway in the postnatal SVZ of the *Cnp*-hEGFR and wild-type mice, mouse brains were electroporated using the ECM 830 BTX electroporator (Harvard Apparatus). Each electroporation result was reproduced in several brains derived from at least three separate litters. SVZ NPC cell depletion using Ara-C (2%, Sigma) in vehicle (0.9% saline) or vehicle alone was performed as described previously[3]. EGF (100 nm μl^{-1}, Upstate) in vehicle (0.9% saline), or vehicle alone was infused into the lateral ventricle of adult *GFAP*–GFP and wild-type mice (infusion coordinates: anterioposterior, 0; lateral, 1.1; dorsoventral, 1.5 mm medial to lateral relative to bregma) for 5 days using micro-osmotic pumps (Alzet, model 1007). Brains were then processed for FACS-purification, cell culture or histology. At least three different brains for each strain and each experimental condition were analysed and counted. Cell counting was performed blindly and tissue sections were matched across samples. The analysis of the SVZ was performed at different anterior-posterior and dorso-ventral levels of the lateral ventricle. Statistical analysis was performed by unpaired *t*-test.

Full Methods and any associated references are available in the online version of the paper at www.nature.com/nature.

Received 6 August 2009; accepted 13 July 2010.

1. Mercier, F., Kitasako, J. T. & Hatton, G. I. Anatomy of the brain neurogenic zones revisited: fractones and the fibroblast/macrophage network. *J. Comp. Neurol.* **451,** 170–188 (2002).
2. Alvarez-Buylla, A. & Lim, D. A. For the long run: maintaining germinal niches in the adult brain. *Neuron* **41,** 683–686 (2004).
3. Doetsch, F., Caillé, I., Lim, D. A., García-Verdugo, J. M. & Alvarez-Buylla, A. Subventricular zone astrocytes are neural stem cells in the adult mammalian brain. *Cell* **97,** 703–716 (1999).
4. Palmer, T. D., Willhoite, A. R. & Gage, F. H. Vascular niche for adult hippocampal neurogenesis. *J. Comp. Neurol.* **425,** 479–494 (2000).
5. Temple, S. The development of neural stem cells. *Nature* **414,** 112–117 (2001).
6. Sundaram, M. V. The love-hate relationship between Ras and Notch. *Genes Dev.* **19,** 1825–1839 (2005).
7. Kumar, J. P. & Moses, K. The EGF receptor and notch signaling pathways control the initiation of the morphogenetic furrow during *Drosophila* eye development. *Development* **128,** 2689–2697 (2001).
8. Yoo, A. S., Bais, C. & Greenwald, I. Crosstalk between the EGFR and LIN-12/Notch pathways in *C. elegans* vulval development. *Science* **303,** 663–666 (2004).
9. Hasson, P. *et al.* EGFR signaling attenuates Groucho-dependent repression to antagonize Notch transcriptional output. *Nature Genet.* **237,** 101–105 (2005).
10. Hitoshi, S. *et al.* Notch pathway molecules are essential for the maintenance, but not the generation, of mammalian neural stem cells. *Genes Dev.* **16,** 846–858 (2002).
11. Alexson, T. O., Hitoshi, S., Coles, B. L., Bernstein, A. & van der Kooy, D. Notch signaling is required to maintain all neural stem cell populations—irrespective of spatial or temporal niche. *Dev. Neurosci.* **28,** 34–48 (2006).
12. Lillien, L. & Raphael, H. BMP and FGF regulate the development of EGF-responsive neural progenitor cells. *Development* **127,** 4993–5005 (2000).
13. Breunig, J. J., Silbereis, J., Vaccarino, F. M., Sestan, N. & Rakic, P. Notch regulates cell fate and dendrite morphology of newborn neurons in the postnatal dentate gyrus. *Proc. Natl Acad. Sci. USA* **104,** 20558–20563 (2007).
14. Aguirre, A., Dupree, J. L., Mangin, J. M. & Gallo, V. A functional role for EGFR signaling in myelination and remyelination. *Nature Neurosci.* **10,** 990–1002 (2007).
15. Aguirre, A., Rizvi, T. A., Ratner, N. & Gallo, V. Overexpression of the epidermal growth factor receptor confers migratory properties to nonmigratory postnatal neural progenitors. *J. Neurosci.* **25,** 11092–11106 (2005).
16. Steiner, B. *et al.* Type-2 cells as link between glial and neuronal lineage in adult hippocampal neurogenesis. *Glia* **54,** 805–814 (2006).
17. Doetsch, F., García-Verdugo, J. M. & Alvarez-Buylla, A. Cellular composition and three-dimensional organization of the subventricular germinal zone in the adult mammalian brain. *J. Neurosci.* **17,** 5046–5061 (1997).
18. Capela, A. & Temple, S. Lex/ssea-1 is expressed by adult mouse CNS stem cells, identifying them as non-ependymal. *Neuron* **35,** 865–875 (2002).
19. Aguirre, A. & Gallo, V. Postnatal neurogenesis and gliogenesis in the olfactory bulb from NG2-expressing progenitors of the subventricular zone. *J. Neurosci.* **24,** 10530–10541 (2004).
20. Jablonska, B. *et al.* Cdk2 is critical for proliferation and self-renewal of neural progenitor cells in the adult subventricular zone. *J. Cell Biol.* **179,** 1231–1245 (2007).
21. Gaiano, N., Nye, J. S. & Fishell, G. Radial glial identity is promoted by Notch1 signaling in the murine forebrain. *Neuron* **26,** 395–404 (2000).
22. Mizutani, K., Yoon, K., Dang, L., Tokunaga, A. & Gaiano, N. Differential Notch signalling distinguishes neural stem cells from intermediate progenitors. *Nature* **449,** 351–355 (2007).
23. Lim, D. A. *et al.* Noggin antagonizes BMP signaling to create a niche for adult neurogenesis. *Neuron* **28,** 713–726 (2000).
24. Colak, D. *et al.* Adult neurogenesis requires Smad4-mediated bone morphogenic protein signaling in stem cells. *J. Neurosci.* **28,** 434–446 (2008).
25. Lai, K., Kaspar, B. K., Gage, F. H. & Schaffer, D. V. Sonic hedgehog regulates adult neural progenitor proliferation *in vitro* and *in vivo*. *Nature Neurosci.* **6,** 21–27 (2003).
26. Kohyama, J. *et al.* Visualization of spatiotemporal activation of Notch signaling: live monitoring and significance in neural development. *Dev. Biol.* **286,** 311–325 (2005).
27. Aguirre, A. & Gallo, V. Reduced EGFR signaling in progenitor cells of the adult subventricular zone attenuates oligodendrogenesis after demyelination. *Neuron Glia Biol.* **3,** 209–220 (2007).
28. McGill, M. A. & McGlade, C. J. Mammalian numb proteins promote Notch1 receptor ubiquitination and degradation of the Notch1 intracellular domain. *J. Biol. Chem.* **278,** 23196–23203 (2003).
29. Chapman, G., Liu, L., Sahlgren, C., Dahlqvist, C. & Lendahl, U. High levels of Notch signaling down-regulate Numb and Numblike. *J. Cell Biol.* **175,** 535–540 (2006).

Supplementary Information is linked to the online version of the paper at www.nature.com/nature.

Acknowledgements We thank N. Ratner for the *Cnp*–hEGFR mice. We are thankful to T. Hawley for technical advice in all FACS sorting experiments. We are grateful to J. Corbin and T. Haydar for critically reading this manuscript, and to all our colleagues at the Center for Neuroscience Research for discussion and support. We are thankful to N. Gaiano for discussion, for providing reagents and for his continuous advice on this project. We thank G. Corfas, A. Israel, C. L. Cepko, R. Kopan, R. Grosschedl, N. Gaiano and R. Kageyama for the gift of CBF-1, *Hes1*–GFP, *Hes1*-dsRED, Notch constructs, *Dll*–GFP, *CBFRE*–EGFP and *Hes5*–GFP, respectively. This work was supported by NIH R01NS045702 and R01NS056427 (V.G.), K99NS057944 (A.A.), ROO NS057944-03 (A.A.) and by NIH IDDRC P30HD40677 (V.G.). Electron microscopy was performed at the University of Connecticut, Department of Physiology and Neurobiology, with funding from NIH R01DC006881 to M.E.R., and from NSF DBI-0420580 for funds to purchase the Tecnai 12 Biotwin electron microscope.

Author Contributions A.A. performed all the experiments. M.E.R. performed the electron microscopy studies. A.A. and V.G. designed all experiments. V.G. supervised the entire project. A.A. and V.G. wrote the manuscript.

Author Information Reprints and permissions information is available at www.nature.com/reprints. The authors declare no competing financial interests. Readers are welcome to comment on the online version of this article at www.nature.com/nature. Correspondence and requests for materials should be addressed to V.G. (vgallo@cnmcresearch.org).

METHODS

Animals. Details on the generation and characterization of *Cnp*–hEGFR transgenic mice have been reported previously[15,30]. Genotyping of the mice was performed by PCR[15]. Robust hEGFR expression was detected in total brain and spinal cord lysates from adult brain by using monoclonal anti-human EGFR antibody to probe western blots after immunoprecipitation with a polyclonal anti-EGFR antibody[14,15,30]. Consistent with the idea that the Cnp promoter drives expression in oligodendrocytes, hEGFR expression was detected in OL lineage cells of the SVZ, white matter and cerebral cortex in P8-P90 Cnp–hEGFR mice, and in $NG2^+$ progenitor cells of the SVZ[15]. Transgenic mice were backcrossed more than four generations onto C57BL/6. In the *Cnp*–hEGFR mouse strain, the *Cnp* promoter drives expression in NPCs and in the entire oligodendrocyte lineage; hEGFR expression was detected at both P8 and P90 in $NG2^+$ progenitors of the SVZ, and in $NG2^+$ progenitors and oligodendrocytes of the white and grey matter[14,15]. The mouse strain expressing the *hGFAP*–EGFP (gift of F. Kirchhoff) was characterized previously[31]. The EGFR-mutant mouse (waved-2 mutation; Wa2)[32] was obtained from Jackson Labs. All animal procedures were performed according to the Institutional Animal Care and Use Committee of the Children's National Medical Center and the National Institutes of Health "Guide for the Care and Use of Laboratory Animals."

Immunohistochemistry and antibodies. Freshly cut, floating tissue sections (20–40 μm) from P8 and P90 mice were prepared as described previously[14,15]. Primary antibody dilutions were 0.5 μg ml^{-1} for the specific anti–hEGFR (Biofluids); 1:500 for anti-BrdU (Accurate), anti-NG2 antibody (Chemicon), monoclonal anti-GFAP (mouse monoclonal, Sigma Aldrich), polyclonal anti-GFAP (rabbit polyclonal, Covance), anti-S100β (DAKO, rabbit anti-human clone A5110), and anti-Nestin (Chemicon); 1:50 for anti-LeX (MMA clone, BD Biosciences), anti-full-length Notch-1, Jagged1, Delta like-1 (Dll) and anti-NICD (from the Developmental Studies Hybridoma Bank).

BrdU administration. The BrdU labelling protocol was performed as described previously[19,33]. The number of proliferating progenitor cells in the subependyma of the lateral ventricle was determined following short-term (2 h), or long-term (30 days) retention. Mice were injected intraperitoneally with a single dose of BrdU (50 μg g^{-1} body weight) every 3 h for five injections and were killed either 1 h or 30 days after the final injection.

Conventional transmission electron microscopy. Wild type and *Cnp*–EGFR mice (P8, $n = 6$ for each phenotype; adult, $n = 4$ for each phenotype) were perfused through the heart with a mixture of 3% paraformaldehyde and 1.25% glutaraldehyde in 0.1 M phosphate buffer. Brains were removed and postfixed overnight with the same fixative. Brains were sectioned with a vibratome and stored in 0.1 M phosphate buffer. Before postfixation for 1 h with 1% osmium tetroxide, slices were washed in 0.1 M cacodylate buffer pH 7.2. After, brain slices were dehydrated through a series of ethanol solutions (50%, 70%, 85%, 95% and 100%), infiltrated with epoxy resins and flat embedded. Sections with the lateral ventricle and the SVZ were trimmed and mounted on blocks and cut with an ultramicrotome. Ultrathin sections (70–80 nm in thickness) were counterstained with uranyl acetate and lead citrate and analysed with a TECNAI G2 Spirit Biotwin TEM (FEI). The images were captured with an AMT XR40 4-megapixel side-mounted CCD camera (Danvers) using the electron micrograph montage option. Image processing was performed with Adobe Photoshop using only the brightness and contrast commands. The identification of cell types in the lateral wall of the lateral ventricle and SVZ was performed on electron micrographs following well-described ultrastructural criteria[17]. Cells were false-coloured and were counted manually.

Microarray and PCR analysis. GEArray expression array systems (catalogue numbers OMM-404MM and OMM-404MM, SuperArray) consisting of spotted cDNA fragments encoding 250 mouse genes involved in NSC development/neurogenesis and in Notch signalling, as well as control sequences (PUC18, glyceraldehyde-3-phosphate dehydrogenase (GAPDH), peptidylpropyl isomerase A (Ppia), and β-actin) were used to compare gene expression between wild-type and *Cnp*–hEGFR SVZ tissue. Total RNA was isolated with the TRIzol method (Invitrogen) and further processed for microarray hybridization according to the manufacturer's instructions. The arrays were visualized by autoradiography and hybridization signals were scanned and analysed for density in GEArray Expression Analysis Suite 2.0. The normalized value for each gene was calculated by dividing the value of each gene by the average value of the housekeeping genes *GAPDH*, *Ppia* and β-actin.

For PCR with reverse transcription, RNA was isolated from P8 and P90 SVZ tissue or from FACS-purified SVZ cells (wild-type and *Cnp–hEGFR* mice), using TRIzol (Invitrogen). RNA (1 μg) from each sample was reverse-transcribed using the SuperScript First-Strand cDNA Synthesis kit (Invitrogen). The mouse gene-specific primers were obtained from Integrated DNA Technologies. Primer sequences for PCR analysis are found in Supplementary Information. Genes were amplified by denaturation at 94 °C for 1 min, annealing at 60 °C for 1 min, and extension at 72 °C for 1 min for 28 cycles. PCR products were resolved by 1.2% agarose gel electrophoresis and visualized by ethidium bromide staining.

***In vivo* electroporation.** For gene transfer into postnatal SVZ cells, *GFAP*–GFP and *GFAP*–GFP/*Cnp*–hEGFR P2-P3 pups were injected with 1–2 μg of pFLAG-NICD (gift from R. Kopan), shhumanEGFR (GeneCopoeia, catalogue number HSH004605-LvH1, access number NM_005228.3; HSHH004605 actcactctccat aaatgc; HSH004605-2 cgtcagcctgaacataaca; HSH004605-3 gaccagacaactgtatcca; HSH004605-4 ccgtcgctatcaaggaatt), *CAG*–GFP and *Hes1*-dsRED and *Hes1*–GFP (gift from C. L. Constance)[34] CBFRE–EGFP (gift from N. Gaiano)[22], *Dll*–GFP (gift from R. Grosschedl)[35] and *Hes5*–GFP (gift from R. Kageyama)[36] DNA into the lateral ventricle, followed by electroporation (100 V/50 ms, five times at 950 ms intervals; the angle of the paddles was adjusted to 20–40 degrees) using an ECM 830 BTX electroporator (Harvard Apparatus).

***In vivo* viral labelling.** SVZ cells were infected using a Notch Intracellular domain (Ad-NICD) or control (Ad-LacZ) construct adenovirus (gift of I. Prudovsky) by direct injection into the lateral ventricle. Adenovirus production and titre determination were previously described[37]. P90 wild-type and *Cnp*–hEGFR mice were injected with the adenovirus stock (2 μl; titre of $2–4 \times 10^6$ plaque-forming units ml^{-1}). Injections were performed stereotaxically at the following coordinates (anterioposterior relative to bregma, mediolateral, and dorsoventral from surface of the brain) for epl-SVZ (0, 1.8, 3.0 mm). Brains were processed for histology at 2, 7, 14 and 28 days after infection, and sections were immunostained for NICD, GFAP, S100b, NG2 and BrdU antibodies.

FACS sorting and cell culture. FACS-purification of $LeX^+NG2^-/EGFP^{neg}$ (NSCs) in the *Cnp*–EGFP mouse or GFAP-$GFP^+LeX^+NG2^{neg}$ (NSCs) in the *GFAP*–GFP mouse has been described previously[19]. Tissue from P8 *Cnp–hEGFR*, *Cnp*–EGFP/*Cnp*–hEGFR, *GFAP*–GFP or *Cnp*–hEGFR/*GFAP*–GFP mice was dissociated into single cell suspensions, followed by immunostaining for NG2 and LeX (MMA clone)[19]. SVZ neural stem cells and NPCs (after EGF or saline infusion, or 5–7 days after focal demyelination of the corpus callosum) were FACS-purified using anti-LeX antibodies to purified LeX^+/*GFAP*–GFP^+ (NSCs) or *GFAP*–$GFP^{neg}LeX^+$ (NPCs) cells from the *hGFAP*–GFP mouse. Tissue was dissociated into single cell suspensions, followed by immunostaining for NG2 and LeX (MMA clone)[19]. To FACS-purify NSCs, antibodies were used in combination with appropriate R-phycoerythrin and PE-Cy5.5-conjugated secondary antibodies (Caltag). Cell suspensions were analysed for light forward and side scatter using a FACSAria instrument (BD Biosciences).

Cultures of FACS-purified cells have been described previously[19]. FACS-purified NSCs were seeded at a density of 10 viable cells per μl on uncoated 24-well plates (BD Falcon), and grown in SCM for 6 days *in vitro* with daily addition of 20 ng ml^{-1} EGF and 10 ng ml^{-1} FGF2 (Upstate)[19,20]. Primary neurosphere colonies were subcloned to assay NSC self-renewal by mechanical dissociation and replated at a density of 10 cells μl^{-1} on uncoated 24-well plates. It is important to note that in Supplementary Fig. 6 neurosphere analysis was performed starting with the second passage. This was done to overcome the experimental limitations due to low number of cells recovered after FACS.

SVZ micro-dissection. SVZ areas were micro-dissected from 300 μm-thick brain coronal sections. Single cell were dissociated[19,38] on coated coverslips in 24-well plates (BD Falcon). Coverslips were processed for immunocytochemistry 2 h after plating.

Western blots and immunoprecipitation. SVZ tissue (wild-type and *Cnp*–hEGFR mice) was micro-dissected from 300-μm-thick coronal sections of P8 and P90 brains, and used for protein extraction using lysis buffer (50 mM Tris-HCl, pH7.5, 1 mM EDTA, 1 mM EGTA, 1 mM sodium orthovanadate, 50 mM sodium fluoride, 0.1% 2-mercaptoethanol, 1% triton X-100, plus proteases inhibitor cocktail; Sigma). Protein samples (20 μg) were separated on GENE Mate express Gels 4–20% (ISC BioExpress) and transferred to PVDF membranes (Millipore). Numb, Notch1, NICD, Dll1, Hes1, RBPjk, ubiquitin and actin proteins, were detected using an enhanced chemiluminescence substrate mixture (ECL Plus, Amersham). Selective primary antibodies from Santa Cruz Biotechnologies were used at 1 μg ml^{-1}. Antibodies were used in combination with a secondary horseradish peroxidase-conjugate (Santa Cruz Biotechnologies).

For immunoprecipitation, SVZ tissue extracts from wild-type and Cnp–hEGFR mice were prepared in RIPA buffer containing 20 mM TrisHCl (pH 7.5), 150 mM NaCl, 1 mM Na_2EDTA, 1 mM EGTA, 1% NP-40, 1% sodium deoxycholate, 2.5 mM sodium pyrophosphate, 1 mM β-glycerophosphate and 1 mM Na_3VO_4. Aliquots (200 μg protein) were incubated overnight with antibodies against ubiquitin (Santa Cruz Biotechnology), Numb or Notch1 and 15 μl of agarose A (Santa Cruz Biotechnology). Immunocomplexes bound to agarose A were collected by centrifugation and washed twice in 500 μl RIPA buffer containing inhibitors. Precipitated proteins were analysed by immunoblotting. Bands were detected using HRP and developed with a chemiluminescent substrate (ECL, Amersham).

Ara-C and EGF infusion. Ara-C (2%, Sigma) in vehicle (0.9% saline) or vehicle alone were infused onto the surface of the brain of adult mice (coordinates: anterioposterior, 0, lateral, 1.1, dorsoventral, 1.5 mm medial to lateral relative to bregma) for 6 days with micro-osmotic pumps (Alzet, model 1007) as described previously[3]. EGF (100 nm μl^{-1}, Upstate) in vehicle (0.9% saline) or vehicle alone was infused into the lateral ventricle in adult *GFAP*–GFP and wild-type mice (infusion coordinates: anterioposterior, 0; lateral, 1.1; dorsoventral, 1.5 mm medial to lateral relative to bregma) for 5 days using micro-osmotic pumps (Alzet, model 1007). Mice were then processed for FACS-purification, cell culture or histology.

Plasmids, siRNAs, cell transfection and luciferase assays. SVZ tissue was dissected from 300-μm-thick brain sections prepared from P8 wild-type and *Cnp–hEGFR* brains and processed for cell culture[19]. After SVZ dissection and single cell dissociation, cells were plated in 12-well cell culture dishes at a density of 50 cells μl^{-1} for 24 h. At the time of transfection, cell cultures were approximately 60% confluent. Cell transfections were performed using the NeuroPORTER Transfection reagent (Genlantis) following manufacturer's instructions. The cell permeable, irreversible EGFR blocker (PD168393, Calbiochem), was used 24 h after cell transfection. Cells were pre-incubated with PD168393 (PD) for 4 h at 37 °C in 5% CO_2 and then medium was changed to fresh SCM.

A commercially available siRNA directed towards the hEGFR was purchased from Dharmacon (SMARTpool catalogue number L-003114-00, locus NM_201283; sequence J-003114-10, CAAAGUGUGUAACGGAAUA; J-003114-11, CCAUAAAUGCUACGAAUAU, J-003114-12, GUAACAAGCUCACGCAGUU, J-003114-13, CAGAGGAUGUUCAAUAACU). siRNA directed towards the mNumb (Santa Cruz Biotechnologies, catalogue number sc-42147; locus NM_010949, 110 GUAGCUUCCCAGUUAAGUAtt, 412 CGAUGGAUCUGU CAUUGUUtt, 884 CCCUACGCAUCAAUGAGUUtt). siRNA transfection produced selective knockdown of the hEGFR and mNumb. Briefly, 2 μl of 20 pM of siRNA solution and 12 μl of the transfection reagent were incubated in 100 μl of SCM for 20 min, in order to facilitate complex formation. The siRNA transfection mix was added to the SVZ cells cultured in 2.5% FBS. Controls consisted of non-specific siRNA. SVZ cells were transfected for 7 h at 37 °C, washed with Hank's buffer and grown in SCM 2.5% FBS for an additional 24 h. The medium was then changed to basal SCM (20 ng ml^{-1} EGF and 10 ng ml^{-1} FGF). After 24 or 48 h, cells were collected and processed for RNA or protein extraction.

Transient transfections and luciferase assays were performed in 60% confluent SVZ cell cultures (*Cnp*–hEGFR and wild type) using NeuroPORTER as described above, and 1.5 μg of PGL3 basic, wild-type phEGFR (Millipore), pCBF1-Luciferase reporter plasmid (gift of G. Corfas) or *Hes1* luciferase reporter plasmid, and Dll expression plasmid (gift of A. Israel) reporter plasmids and 0.3 μg of expression vectors. Notch expression vectors used were a gift of R. Kopan. Luciferase assays were performed 48 h after transfection using the Dual Assay Luciferase kit (Promega). Cotransfected thymidine kinase–*Renilla* luciferase was used to normalize samples for transfection efficiency and for sample handling. Cells were lysed, and luciferase activity was measured following the protocol recommended by the manufacturer.

Neural progenitor–neural stem cell co-cultures. NPCs were acutely dissociated from P8 *Cnp*–hEGFR and wild-type SVZ mice and then processed for purification using anti-prominin-1 microbeads antibodies (Miltenyi Biotec) following manufacturer recommendations. Purified NPCs were cultured at high density in a monolayer in the presence of EGF and FGF2, as described above. After 48 h, FACS-purified wild-type *GFAP*–GFP^+LeX^+ cells were plated on top of NPCs for 5 days in EGF- and FGF2-containing medium. Finally, *GFAP*–GFP^+ cells were purified from the co-culture by FACS and assayed in neurosphere cultures to determine proliferation and self-renewal. FACS-purified *GFAP*–GFP^+ cells were seeded at a density of 5 viable cells per μl on uncoated 12 mm-well plates (BDFalcon), and maintained in SCM for 6 days *in vitro* with daily addition of EGF and FGF2. Primary neurosphere colonies were subcloned by mechanical dissociation in SCM with EGF and FGF2. Cells were re-plated at a density of 5 cells per μl on uncoated 24-well plates. Stem cell self-renewal was assessed after further 6 days *in vitro*.

Microscopy and cell counting. A Bio-Rad MRC 1024 confocal laser-scanning microscope equipped with a krypton-argon laser and an Olympus IX-70 inverted microscope was used to image localization of FITC (488 nm laser line excitation; 522/35 emission filter), texas red (568 nm excitation; 605/32 emission filter) of Cy5 (647 excitation; 680/32 emission filter). Optical sections ($Z = 0.5\mu m$) of confocal epifluorescence images were acquired sequentially using a ×40 oil objective (number of aperture, NA = 1.35), or a ×60 oil objective (NA = 1.40) with Bio-Rad LaserSharp v3.2 software. ImageJ NIH software was subsequently used to merge images. Merge images were processed in Photoshop 7.0 with minimal manipulations of contrast. Cells were counted in the SVZ the postnatal day 8 (P8) and adult mice P90. At least three different brains for each strain and each experimental condition were analysed and counted. Cell counting was performed blindly and tissue sections were matched across samples. The analysis of the SVZ was performed at different anterior-posterior and dorso-ventral levels of the lateral ventricle. An average of 15–20 sections was quantified using unbiased stereological morphometric analysis for the SVZ to obtain an estimate of the total number of positive cells. Then, percentages of cells expressing different antigens were estimated by scoring the number of cells double-labelled with the marker in question. In acute SVZ dissociated cells, three coverslips and 8–10 microscopic fields/coverslip were counted from three separate cultures. Statistical analysis was performed by unpaired *t*-test.

30. Ling, B. C. *et al.* Role for the epidermal growth factor receptor in neurofibromatosis-related peripheral nerve tumorigenesis. *Cancer Cell* **7**, 65–75 (2005).
31. Wehner, T. *et al.* Bone marrow-derived cells expressing green fluorescent protein under the control of the glial fibrillary acidic protein promoter do not differentiate into astrocytes *in vitro* and *in vivo*. *J. Neurosci.* **23**, 5004–5011 (2003).
32. Luetteke, N. C. *et al.* The mouse waved-2 phenotype results from a point mutation in the EGF receptor tyrosine kinase. *Genes Dev.* **8**, 399–413 (1994).
33. Morshead, C. M., Craig, C. G. & van der Kooy, D. *In vivo* clonal analyses reveal the properties of endogenous neural stem cell proliferation in the adult mammalian forebrain. *Development* **125**, 2251–2261 (1998).
34. Matsuda, T. & Cepko, C. L. Controlled expression of transgenes introduced by *in vivo* electroporation. *Proc. Natl Acad. Sci. USA* **104**, 1027–1032 (2007).
35. Galceran, J., Sustmann, C., Hsu, S. C., Folberth, S. & Grosschedl, R. LEF1-mediated regulation of Delta-like1 links Wnt and Notch signaling in somitogenesis. *Genes Dev.* **18**, 2718–2723 (2004).
36. Ohtsuka, T. *et al.* Visualization of embryonic neural stem cells using Hes promoters in transgenic mice. *Mol. Cell. Neurosci.* **31**, 109–122 (2006).
37. Kolev, V. *et al.* The intracellular domain of Notch ligand Delta1 induces cell growth arrest. *FEBS Lett.* **579**, 5798–5802 (2005).
38. Belachew, S. *et al.* Postnatal NG2 proteoglycan-expressing progenitor cells are intrinsically multipotent and generate functional neurons. *J. Cell Biol.* **161**, 169–186 (2003).